Atmos. Chem. Phys. Discuss., 12, 9985–10014, 2012
www.atmos-chem-phys-discuss.net/12/9985/2012/
doi:10.5194/acpd-12-9985-2012

Atmospheric Chemistry and Physics Discussions

CO_2 flux estimation errors associated with moist atmospheric processes

N. C. Parazoo[1], A. S. Denning[2], S. R. Kawa[3], S. Pawson[3], and R. Lokupitiya[4]

[1]Jet Propulsion Laboratory, California Institute of Technology, Pasadena, CA, USA
[2]Department of Atmospheric Science, Colorado State University, Fort Collins, Colorado, USA
[3]NASA Goddard Space Flight Center, Greenbelt, Maryland, USA
[4]Department of Statistics and Computer Science, University of Sri Jawawardenepura, Gangodawila, Nugegoda, Sri Lanka

Received: 3 April 2012 – Accepted: 3 April 2012 – Published: 18 April 2012

Correspondence to: N. C. Parazoo (nicholas.c.parazoo@jpl.nasa.gov)

Published by Copernicus Publications on behalf of the European Geosciences Union.

Abstract

Vertical transport by moist sub-grid scale processes such as deep convection is a well-known source of uncertainty in CO_2 source/sink inversion. However, a dynamical link between moist transport, satellite CO_2 retrievals, and source/sink inversion has not yet been established. Here we examine the effect of moist processes on (1) synoptic CO_2 transport by Version-4 and Version-5 NASA Goddard Earth Observing System Data Assimilation System (NASA-DAS) meteorological analyses, and (2) source/sink inversion. We find that synoptic transport processes, such as fronts and dry/moist conveyors, feed off background vertical CO_2 gradients, which are modulated by sub-grid vertical transport. The implication for source/sink estimation is two-fold. First, CO_2 variations contained in moist poleward moving air masses are systematically different from variations in dry equatorward moving air. Moist poleward transport is hidden from orbital sensors on satellites, causing a sampling bias, which leads directly to continental scale source/sink estimation errors of up to 0.25 PgC yr^{-1} in northern mid-latitudes. Second, moist processes are represented differently in GEOS-4 and GEOS-5, leading to differences in vertical CO_2 gradients, moist poleward and dry equatorward CO_2 transport, and therefore the fraction of CO_2 variations hidden in moist air from satellites. As a result, sampling biases are amplified, causing source/sink estimation errors of up to 0.55 PgC yr^{-1} in northern mid-latitudes. These results, cast from the perspective of moist frontal transport processes, support previous arguments that the vertical gradient of CO_2 is a major source of uncertainty in source/sink inversion.

1 Introduction

Measurements of CO_2 mixing ratio contain information about land and ocean carbon sinks, which act as natural buffers against rising fossil fuel emissions. Flux inversion methods combine information from winds, CO_2 measurements, and surface flux estimates to infer the size and distribution of these sinks (e.g. Gurney et al.,

ACPD
12, 9985–10014, 2012

2002). Continuous records residing in the continental boundary layer close to terrestrial ecosystems have allowed quantitative flux estimation at finer special scales then previously possible (e.g. Law et al., 2003; Peylin et al., 2005; Zupanski et al., 2007; Lauvaux et al., 2008; Schuh et al., 2010). Model transport error, specifically related to sub-grid scale vertical transport, is a well-known but poorly characterized source of uncertainty (Denning et al., 1999; Yi et al., 2004; Yang et al., 2007; Stephens et al., 2007; Liu et al., 2011). Surface and space-based measurements of column-integrated CO_2, which are critical for filling spatial gaps in the in-situ network, are also prone to transport error (Baker et al., 2010; Houweling et al., 2010; Chevallier et al., 2010, 2011).

In the era of satellite measurements, an additional complication arises because the strongest horizontal gradients in CO_2 occur along frontal boundaries that are typically hidden from orbital sensors by clouds (Corbin et al., 2006), leading to systematic sampling errors of up to 1.5 ppm at seasonal scales (Corbin et al., 2008). Because a significant portion of the synoptic signal is correlated with moist processes and therefore likely to be unobserved by satellites (Parazoo et al., 2011), covariance of moist transport with surface CO_2 flux will cause errors in top-down flux estimates if not represented correctly in transport models.

In this study we quantify differences in forward calculations of moist frontal CO_2 transport and the resulting impact on inverse flux estimates. Forward simulations are run using a common tracer transport model and identical surface fluxes, but with transport driven by four reanalysis products from NASA GEOS-DAS. The four resulting simulations are analyzed in terms of eddy and mean meridional mass fluxes of CO_2 using eddy decomposition (Parazoo et al., 2011), where the eddy term is a proxy for frontal CO_2 transport. Uncertainty in frontal transport is quantified as model spread in eddy transport (in units of PgC month^{-1}).

Transport uncertainty is interpreted through model differences grid spacing and the representation of sub-grid scale vertical mixing. Unique aspects of forward simulations include the use of (1) an identical tracer model and surface fluxes, (2) meteorological analyses derived from a common general circulation model (GCM), and (3) a novel

ACPD
12, 9985–10014, 2012

eddy decomposition approach for analyzing meridional transport by synoptic storms. Conversely, intercomparison studies that use a wider set of models are unable to account for sensitivity due to differences in dynamical core, meteorology, coordinate systems, and surface fluxes. While most forward simulations of CO_2 will have flaws, here we are at least able to account for sensitivity to an isolated set of factors.

We also examine sensitivity of flux inversions to moist frontal transport using Observation System Simulation Experiments, or OSSE's. Several OSSE's are presented in order to separate errors in technique (e.g. ensemble approximation) from errors in transport. The approach for each OSSE has two primary steps: (1) the nature run, in which synthetic retrievals of column CO_2 are created by propagating realistic looking CO_2 fluxes (henceforth the "true" flux) through a tracer transport model to produce seasonally varying CO_2, which is then sampled along the Greenhouse gases Observing SATellite (GOSAT) orbit (e.g. Kuze et al., 2009), and (2) the full flux inversion run, in which true fluxes are recovered from synthetic retrievals using ensemble optimization.

OSSEs are similar in design to Chevallier et al. (2010), where one set of experiments uses the same meteorological analysis for transport in Steps 1 and 2, and another set examines transport bias by using different meteorological analysis in Steps 1 and 2. Several key differences are as follows: (1) the current study uses the same transport model in all experiments and varies only in the meteorological dataset, eliminating sensitivity to differences in numerical integration; (2) very similar (in architecture) but systematically different (in physics) meteorological datasets are used; (3) use of ensemble data assimilation framework and estimation of systematic biases to component fluxes (technique described in Lokupitiya et al. (2008) and references therein); (4) end-to-end OSSE's are performed to quantify baseline errors in the inversion system, in particular due to temporal sampling errors, before errors related to transport uncertainty are analyzed; and (5) more attention is given to sensitivity of flux estimates to model differences in vertical mixing and eddy CO_2 transport. This last point is key: rather than point out when and where flux estimation errors occur, we attempt to explain flux errors from

ACPD
12, 9985–10014, 2012

a dynamical viewpoint. Given the similarity of experiments yet uniqueness of methods, Chevallier et al. (2010) provide an excellent benchmark for comparison.

2 Methods

2.1 Forward simulations

CO_2 transport is analyzed in the global Parameterized Chemistry and Transport Model (PCTM, see Kawa et al., 2004). Surface fluxes, described in Parazoo et al. (2008), are the same for each simulation, and include air-sea exchange, constant in time fossil fuel emissions, and a steady state terrestrial biosphere. These fluxes are also used as "priors" in Step 2 of the source/sink inversion experiments (see Sect. 2.2). PCTM is run from 1 January 2000 through 31 December 2004 to spin up atmospheric gradients of CO_2 and create a common initial condition, and from 1 January 2005 through 31 December 2005 using the four reanalysis products (described below) to comprise the analysis period.

Transport in the PCTM is computed off-line using archived meteorological analyses from different versions of the GEOS DAS. Two distinctly different GEOS analyses, Versions 4 and 5, are used in this study. These meteorological analyses differ in (1) physical parameterizations in the GCM, (2) native resolution, (3) the algorithm used for the meteorological analysis, and (4) the manner in which the analyses are assimilated with the GCM. The physical parameterizations in the GEOS-4 GCM are substantially different from GEOS-5 (see below). GEOS-4 has a native resolution of $1.25^\circ \times 1^\circ$ (longitude × latitude) and 55 layers while GEOS-5 is "better resolved" at $0.67^\circ \times 0.5^\circ$ and 72 layers. Most of the additional layers in GEOS-5 are in the troposphere. This study uses meteorological datasets saved at the native resolution of each of these forecast models. We also use two additional datasets that are saved at a reduced resolution, giving a total of four meteorological datasets based on the same dynamical core to transport CO_2. The different analysis techniques are likely to impact simulations, but

ACPD
12, 9985–10014, 2012

isolating this factor is difficult in an offline framework. We therefore focus on the impact of horizontal grid spacing and sub-grid transport on forward simulations of CO_2 transport, keeping in mind sensitivity to other factors. The key differences between these models are summarized in Table 1 and specified in more detail below.

The GEOS-4 analysis (Bloom et al., 2005) procedure uses the Physical-space Statistical Analysis Scheme of Cohn et al. (1998), which produces an optimal combination of six-hour model forecasts and observations at the observation locations. These are interpolated to the model grid and the model background fields (surface pressure, winds, temperature and moisture) are replaced with the analyses every six hours. Six-hour time-averaged GEOS-4 fields are used in the present study (Pawson et al., 2007). Physical parameterizations in GEOS-4 are drawn from the National Center for Atmospheric Research Community Climate Model, Version 3 (CCM3) package (Kiehl et al., 1998), which include deep convection (Zhang and McFarlane, 1995), shallow convection (Hack, 1994), and PBL turbulence (Holtslag and Boville, 1993).

GEOS-5 analyses (Rienecker et al., 2008) use a three-dimensional variational approach in gridpoint space (Gridpoint Statistical Analysis, GSI; Wu et al., 2002) that directly assimilates satellite radiances alongside the conventional meteorological data. These analyses are input smoothly into the GEOS-5 GCM, using the incremental analysis update (IAU) approach of Bloom et al. (1996): this involves adding additional forcing terms to the momentum, thermodynamic and moisture tendencies, which are the local (gridpoint) forces needed to drive the background forecasts to the analyses over the six-hour window of the assimilation. This method of merging the analyses to the model leads to smoothly varying fields in the assimilation, which means that the transport in GEOS-5 is much smoother than in GEOS-4, and does not require time averaging. The GEOS-5 GCM maintains the finite-volume dynamics used in GEOS-4 (Lin, 2004) and is integrated with physics packages under the Earth System Modeling framework (e.g. Collins et al., 2005), including the Relaxed Arakawa-Schubert (RAS) scheme for convection (Moorthi and Suarez, 1992) and separate PBL turbulent mixing schemes for stable (Louis et al., 1982) and unstable (Lock et al., 2000) conditions.

ACPD
12, 9985–10014, 2012

2.1.1 G4F10

The first analysis used in this study is the GEOS-4 DAS, as used by Kawa et al. (2004) in the original PCTM study of CO_2 transport. GEOS-4 DAS transport fields are saved at 6-hourly resolution and 1.25° by 1° (the native resolution of GEOS-4 DAS) grid spacing with 55 hybrid vertical levels up to 0.01 hPa. This re-analysis driver data will be referred to as G4F10. Of the 55 vertical levels, only 14 are located within the troposphere. Since the mixing time scale between the troposphere and stratosphere is approximately 10 yr, and this study is focused on processes in the troposphere at time scales much less than 10 yr, the 55 vertical levels in G4F10 are condensed to 25 levels while retaining all levels in the troposphere. 1.25° by 1° transport in PCTM is run with a 7.5 min time step.

2.1.2 G4R20

G4F10 is regridded horizontally to 2.5° by 2° to study transport at coarser horizontal resolution. Vertical mixing by moist convection and turbulent diffusion is identical to G4F10. Wind vectors are also conserved, but regridding to coarser resolution has smoothed spatial gradients. All 25 vertical levels are retained, and transport fields are still saved at 6-hourly resolution. Time-stepping through PCTM is doubled to 15 min. This regridded re-analysis is referred to as G4R20.

2.1.3 G5F05

The third product is based on version 5 of GEOS-DAS (GEOS-5 DAS, Rienecker et al., 2008). Aside from different native spatial resolution, the sub-grid vertical mixing schemes in GEOS-5 are a key difference between GEOS-4 and GEOS-5. The effect of these schemes on CO_2 transport is unfortunately not separable from that of grid spacing. This first GEOS-5 product is from Version 5.1.0, which was run for the period 1 October 2003–2 October 2008 in support of NASA's science missions. The native grid of GEOS-5 DAS (the grid at which the analysis is performed) is 0.67° by 0.5°

ACPD
12, 9985–10014, 2012

in the horizontal with 72 layers to 0.01 hPa, 31 of which are in the troposphere. The 72 vertical layers are reduced to 42 levels while retaining the 31 tropospheric levels. Instantaneous transport fields are saved at 6-hourly resolution. Reduced grid spacing requires a time step of 3.75 min. This driver data is referred to as G5F05.

2.1.4 G5R10

The fourth product is similar to G5F05 except with a newer version (5.2.0) of GEOS-5 DAS used for the Modern-Era Retrospective analysis for Research Applications (MERRA) (Rienecker et al., 2011). The system contains several improvements from the GEOS-5.1.0 system (Rienecker et al., 2008), including tuning of the sub-grid physical packages and aspects of the GSI analysis system. Transport fields are re-analyzed (saved during a corrector segment of the Incremental Analysis Update rather than the analysis segment) and saved every 3 h at a reduced horizontal resolution of 1.25° by 1°. This facilitates comparison with the G4F10 dataset, although it should be noted that analyses with GEOS-5 performed at the 1.25° by 1° resolution differ in important ways from the data that are interpolated to that resolution. This re-analyzed driver data will be referred to as G5R10.

2.2 Synthetic inversion experiments

The inversion system uses the Maximum Likelihood Ensemble System (MLEF) for optimization (Zupanski et al., 2007; Lokupitiya et al., 2008). The strategy for flux estimation is based on the idea that high frequency variations in respiration and photosynthesis are driven by relatively well-understood and easily modeled processes that are determined to first order by variations in solar radiation (Zupanski et al., 2007), while slowly varying processes (e.g. nitrogen deposition) are typically not modeled as well and lead to persistent biases in CO_2 exchange. We therefore prescribe hourly, synoptic, and seasonal variations in terrestrial CO_2 flux and allow the inversion to solve for persistent biases. Lokupitiya et al. (2008) solved for 8-week biases using synthetic data based

ACPD
12, 9985–10014, 2012

on the in-situ network. Here we use synthetic satellite data based and allow biases to persist for 2 weeks due to improved spatial coverage.

Synthetic satellite data is sampled in PCTM according to GOSAT, which uses a sun-synchronous orbit with early afternoon sun-lit equator crossing time (~01:30 p.m. local time) and orbital inclination near 98°. Since GOSAT measures O_2 absorption using reflected solar radiation, the transport model is sampled only during daytime during the descending mode of the orbit. Subsequent orbits are separated by ~25° in longitude and ~99 min apart. GOSAT points near-nadir as well as at the sun glint spot, which greatly increases the signal over the ocean. We assume a 5-point cross-scan track, which was used on GOSAT between 4 April 2009 and 31 July 2010, with footprints separated by ~158 km cross-track and ~152 km along track (Crisp et al., 2012). A maximum of 281 points are sampled by GOSAT in one hour, corresponding to 94 416 points over the 2-week assimilation period. The number of samples over land is much larger than over ocean because of cross-scans, and all possible glint retrievals are retained, including those beyond ±20° of latitude from solar declination, even though these are not collected in reality by GOSAT. We assume GOSAT retrievals have uncertainty of 3 ppm, which is chosen as an upper bound from values computed by Chevallier et al. (2009) due to measurement noise, smoothing error, interference error component, and overall random contribution of aerosols to retrieval noise.

Clear conditions are defined as grid cells with cloud optical depth less than 0.3. Aerosol effects are not considered in this study. Cloud optical depth is prescribed from MERRA and defined as the grid scale value (total in-cloud optical depth from ice and liquid water times the three dimensional total cloud fraction in a grid box). MERRA estimates of clear-sky ratio compare favorably with CALIOP estimates from Eguchi and Yokota (2008) in northern middle and boreal latitudes and in tropical regions. MERRA tends to overestimate the percentage of clear sky days in southern Africa, Australia, the mid-continental portion of southern S. America near 30° S, over the Southern Ocean, and the Arctic. Cloud screening leads to greater than 90 % loss of data in many cases, especially in persistent cloudy areas such as tropical and boreal latitudes.

ACPD
12, 9985–10014, 2012

A total of six OSSE's are reported in this study (see Table 2). OSSE's 1 and 2 are "perfect transport" experiments, where the same meteorological dataset, G4R20, is used in Steps 1 and 2. These experiments are simplified further in that the true flux consists of a steady state terrestrial biosphere, and are therefore designed to establish baseline flux estimation errors due to ensemble optimization, random measurement error, measurement density reduction due to cloud screening, and temporal sampling biases. OSSE's 3 and 4 are "signal detection" experiments, where the true flux includes the steady state terrestrial biosphere plus a slowly varying and globally distributed 3 GtC sink. This sink represents the persistent bias in the steady state terrestrial biosphere as described above and in Zupanski et al. (2007). These experiments are therefore designed to test whether slowly varying sinks due to poorly modeled processes such as nitrogen deposition and regrowing forests in northern middle latitudes and CO_2 fertilization in the tropics are recovered from synthetic satellite retrievals. OSSE's 5 and 6 are "biased transport" experiments, designed to quantify transport-driven flux errors that arise when using G5R05 in Step 1.

3 Results

3.1 Transport differences

Column integrated meridional CO_2 transport is shown in Fig. 1. Total column transport is approximately conserved between meteorological reanalysis. In the annual average, there is net northward transport north of 50° N and net southward transport south of 50° N (Fig. 1a); this pattern is dominated by winter transport (Fig. 1b). The direction of eddy and mean CO_2 transport is independent of reanalysis. Eddy transport is on average poleward in both hemispheres and opposed by southward mean transport in northern latitudes. The direction of eddy and mean transport switches sign in summer north of 50° N (Fig. 1c), consistent with strong CO_2 uptake. The magnitude of transport by eddy and mean circulations is, however, quite sensitive to the reanalysis. For

ACPD
12, 9985–10014, 2012

example, eddy transport in northern mid-latitudes (40–60° N) is generally stronger and more poleward in GEOS-5, exceeding transport in GEOS-4 by 0.1 PgC month^{-1} in the annual mean and close to 0.2 PgC month^{-1} during winter and summer.

GEOS-4 models differ only in horizontal grid spacing; transport differences between G4R20 and G4F10, although small, are therefore explained by regridding of G4F10 to the coarser grid of G4R20. Different transport in GEOS-5 models is also largely explained by differences in grid spacing, although data assimilation procedures and model physics updates between 5.1.0 and 5.2.0 (e.g. high latitude diurnal cycle) may also contribute. Transport differences between G4F10 and G5R10 are more complicated, and likely due to a combination of (1) the representation of sub-grid scale processes, (2) horizontal/vertical grid spacing, (3) the new data assimilation system and (4) number and type of observational data assimilated.

Sub-grid scale processes are probably easiest to examine because mass flux coefficients for cumulus convection and turbulent diffusion are saved in the reanalysis. Vertical mass fluxes are plotted as a function of the terrain following coordinate η and averaged in northern mid-latitudes (30–70° N) in Fig. 2. Turbulent mixing (Fig. 2a) and cumulus convection (Fig. 2b) in GEOS-5 are consistently weaker than GEOS-4 throughout the column in northern mid-latitudes. Weak vertical mixing in mid-latitudes in GEOS-5 is consistent with Ott et al. (2009), who found that single column model application of RAS significantly underestimates convective mass flux relative to cloud resolving models for several case studies of mid-latitude convective storms, resulting in weaker vertical transport of trace gases. The findings of Ott et al. (2009) were subsequently used to tune several key parameters in the convective parameterization of the GEOS-5 GCM. The effect of the tuning is apparent in the newer version of GEOS-5 (i.e. G5R10), where the vertical convective mass flux is larger than G5F05 in mid-latitudes while preserving the vertical distribution. Weaker vertical mixing in GEOS-5 traps CO_2 near the surface (Fig. 2c), causing a stronger negative (positive) vertical CO_2 gradient in the lower troposphere ($\eta = 1 - 0.9$) in the annual (summer) average. Since cold fronts and moist conveyors embedded in synoptic storms move CO_2 upward and poleward

ACPD
12, 9985–10014, 2012

(Parazoo et al., 2011), it follows that stronger vertical gradients in GEOS-5 enhance poleward eddy CO_2 transport.

Differences in meridional wind associated with the combined (and non-linear) effects of sub-grid vertical transport, grid spacing, and data assimilation (Fig. 3) also cause differences in eddy CO_2 transport. Meridional mass fluxes in GEOS-4 and GEOS-5 have similar spatial patterns during boreal summer in northern mid-latitudes, but have regional differences in magnitude, especially in in regions of equatorward transport (blue shading). With the exception of enhanced poleward transport in eastern Europe (25–50° E), equatorward and poleward mass fluxes are typically weaker in GEOS-5. Nevertheless, eddy CO_2 transport is generally stronger in GEOS-5 throughout mid-latitudes (Fig. 4), suggesting that enhanced vertical CO_2 gradients associated with weaker sub-grid vertical mixing are the primary driver of enhanced eddy CO_2 transport in GEOS-5.

3.2 Source/sink inversion

The effect of differences in eddy transport on inverse flux estimates is tested in the following series of inversion experiments, starting with simplified "perfect transport" experiments. First, when all retrievals are retained (Experiment 1), we find that total annual flux errors, representing the difference between the recovered and true flux, are negligible ($<0.1\,\mathrm{PgC\,yr^{-1}}$, Fig. 5a, dark blue) and initial uncertainty is reduced by 50 % (Fig. 5b), indicating MLEF inversion is robust to numerical errors. Seasonal errors are also small and mostly random (e.g. Fig. 6a). These baseline errors are not sensitive to the initial distribution of ensembles or ensemble size (50–200 ensembles), and do not increase when synthetic retrievals are randomly screened. For example, removal of 67 % of data using a random filter produces spatial patterns similar to Fig. 6a.

Screening specifically for retrievals with cloud optical depth greater than 0.3 (Experiment 2) also eliminates more than 67 % of observations in many regions; however, such systematic screening leads to flux errors of up to $0.25\,\mathrm{PgC\,yr^{-1}}$ in the tropics and $0.2\,\mathrm{PgC\,yr^{-1}}$ in Europe (Fig. 5, medium blue), which in northern mid-latitudes are most

ACPD
12, 9985–10014, 2012

prominent during boreal summer (Fig. 6b). Results from Experiments 1 and 2 suggest that flux errors are more sensitive to the type, in contrast to quantity, of data removed.

Summertime flux errors in Europe and N. America (Fig. 6b) tend to be distributed in a way that aligns with patterns of poleward eddy CO_2 transport by G4R20 (Fig. 4a). For example, high CO_2 air is transported into the east half of N. America during summer through two mechanisms: upward and poleward moving moist conveyors in the south (red shading in the Southeast), which advect high CO_2 sub-tropical air residing in the lower troposphere, and downward and equatorward moving dry air intrusions from the north, which advect high CO_2 arctic air from the upper troposphere. Plots of column integrated meridional mass flux illustrate these air streams (Fig. 3a). While equatorward-moving air masses are typically dry and well sampled by satellites, poleward-moving air is moist and cloudy, causing an estimated 30 % of the underlying CO_2 air mass to be hidden in clouds from satellites (Parazoo et al., 2011), causing a temporal sampling bias in the absence of surface observations. Although both air masses are high in CO_2, equatorward transport from the north is stronger. The air sampled by satellites is therefore enriched in CO_2 relative to average conditions, and the inversion compensates by creating a CO_2 "source" over N. America. A similar process of strong poleward transport of high CO_2 air in moist conveyors is responsible for the summer "source" in eastern Europe.

Despite these sampling biases, 80 % of the global 3.0 GtC sink represented by slowly varying processes in middle and tropical latitudes is recovered (Experiment 3, Fig. 5, cyan). Perturbing the sinks with spatial noise and seasonality does not degrade recovery (Experiment 4, Fig. 5, yellow). The inversion also recovers the spatial distribution of sinks in N. America and tropical regions (Fig. 7). While the effect of the temporal sampling bias is clear in Europe, and reduces sink recovery in N. America, Experiments 3 and 4 illustrate that the bias recovery approach can separate slowly varying signals contained in column integrated CO_2 from high frequency signals, and then attribute these signals to the correct processes.

ACPD
12, 9985–10014, 2012

The next set of inversion experiments use G5F05 to create synthetic satellite retrievals and therefore have "biased" transport. As a result, flux errors increase significantly from baseline errors in perfect transport experiments (Experiment 5 in Figs. 3 and 8a). In the case of S. America, flux errors change sign (Fig. 8). We find a global land source of $0.94 \pm 1.23\,\mathrm{GtC\,yr^{-1}}$, with Europe ($0.55 \pm 0.25\,\mathrm{GtC\,yr^{-1}}$), Eurasian Temperate ($0.32 \pm 0.23\,\mathrm{GtC\,yr^{-1}}$), and S. America Tropical ($0.21 \pm 0.71\,\mathrm{GtC\,yr^{-1}}$) contributing most significantly. The global land source increases to $1.4\,\mathrm{PgC\,yr^{-1}}$ when slowly varying sinks are added (Experiment 6 in Fig. 5). These errors are consistent with Chevallier et al. (2010). Relative to Experiments 1–4, the European source is strongly amplified while N. America becomes a sink.

Differences in eddy transport amplify temporal sampling bias in Europe and reverse the sign of bias in N. America. During N. America summer, G4F05 reduces poleward mass flux in the south (relative to G4R20) and equatorward mass flux in the north (Fig. 3c). While both processes decrease transport of high CO_2 into N. America, reduction of equatorward transport of high CO_2 air exceeds reduction of poleward transport (blue shading in N. America, Fig. 4c). As a result, synthetic satellite data is depleted in CO_2, in contrast to Experiment 2, and the inversion creates a "sink" over N. America. Meanwhile, poleward mass fluxes, and hence poleward eddy CO_2 transport, is enhanced in eastern Europe in G5F05. This amplifies the fraction of high CO_2 air hidden from satellites and therefore amplifies the "source" found in Experiment 2.

4 Conclusions

Upward and poleward frontal CO_2 transport feeds off the background vertical CO_2 gradient, which is modulated by sub-grid vertical transport processes such as cumulus convection and turbulent diffusion. Air masses transport by frontal processes are moist, and contain systematically different CO_2 signals from equatorward-moving dry air masses. The implication for source/sink estimation is two-fold. First, CO_2 signals contained in moist air masses are hidden from orbital sensors on satellites and

ACPD
12, 9985–10014, 2012

therefore cause specific errors in source/sink estimation in northern mid-latitudes, up to 0.25 PgC yr^{-1} at continental scales. Second, moist processes are represented differently in GEOS-4 and GEOS-5, leading to differences in the vertical CO_2 gradient and hence the fraction of moist CO_2 air hidden from satellites. As a result, flux estimation errors are amplified (in some cases reversed), causing errors of up to 0.55 PgC yr^{-1} at continental scale and 1.4 PgC at global scale, representing nearly half of the global land sink. These results, cast from the perspective of moist frontal transport processes, support previous arguments that the vertical gradient of CO_2 is a major cause of errors in source/sink inversions.

There is little doubt in the CO_2 inversion community that priority should be given to improving the representation of sub-grid vertical transport. This will however take time, and until transport processes improve, techniques to alleviate the effect of transport errors exist. Joint inversion of column and surface CO_2 data helps (Chevallier et al., 2011). Other approaches involve implicitly accounting for transport errors using a Monte Carlo approach (Chavallier et al., 2007), running ensembles of meteorological analysis fields (e.g. Liu et al., 2011), in particular accounting for uncertainty in sub-grid scale vertical mixing (Teixeira et al., 2008), and assimilated meteorological and CO_2 observations into an ensemble inversion system (Kang et al., 2011).

Acknowledgements. This research is supported by NASA Carbon Cycle Science and NASA grants NNX08AM56G and MAP/04-0085-0081.

ACPD
12, 9985–10014, 2012

References

Baker, D. F., Bösch, H., Doney, S. C., O'Brien, D., and Schimel, D. S.: Carbon source/sink information provided by column CO_2 measurements from the Orbiting Carbon Observatory, Atmos. Chem. Phys., 10, 4145–4165, doi:10.5194/acp-10-4145-2010, 2010.

Bloom, S. C., Takacs, L. L., Da Silva, A. M., and Ledvina, D.: Data assimilation using incremental analysis updates, Mon. Weather Rev., 124, 1256–1271, 1996.

Bloom, S., da Silva, A., and Dee, D.: Documentation and Validation of the Goddard Earth Observing System (GEOS) Data Assimilation System – Version 4. Technical Report Series on Global Modeling and Data Assimilation, in Global Modeling Data Assimilation 104606, Tech. Rep. Ser. 26, NASA Goddard Space Flight Cent., Md., 2005.

Chevallier, F., Breon, F.-M., and Rayner, P. J.: Contribution of the Orbiting Carbon Observatory to the estimation of CO_2 sources and sinks: Theoretical study in a variational data assimilation framework, J. Geophys. Res., 112, D09307, doi:10.1029/2006JD007375, 2007.

Chevallier, F., Maksyutov, S., Bousquet, P., Breon, F.-M., Saito, R., Yoshida, Y., and Yokota, T.: On the accuracy of the CO_2 surface fluxes to be estimated from the GOSAT observations, Geophys. Res. Lett., 36, L19807, doi:10.1029/2009GL040108, 2009.

Chevallier, F., Feng, L., Boesch, H., Palmer, P., and Rayner, P.: On the impact of transport model errors for the estimation of CO_2 surface fluxes from GOSAT observations, Geophys. Res. Lett., 37, L21803, doi:10.1029/2010GL044652, 2010.

Chevallier, F., Deutscher, N. M., Conway, T. J., Ciais, P., Ciattaglia, L., Dohe, S., Fröhlich, M., Gomez-Pelaez, A. J., Griffith, D., Hase, F., Haszpra, L., Krummel, P., Kyrö, E., Labuschagne, C., Langenfelds, R., Machida, T., Maignan, F., Matsueda, H., Morino, I., Notholt, J., Ramonet, M., Sawa, Y., Schmidt, M., Sherlock, V., Steele, P., Strong, K., Sussmann, R., Wennberg, P., Wofsy, S., Worthy, D., Wunch, D., and Zimnoch, M.: Global CO_2 fluxes inferred from surface air-sample measurements and from TCCON retrievals of the CO_2 total column, Geophys. Res. Lett., 38, L24810, doi:10.1029/2011GL049899, 2011.

Cohn, S. E., Da Silva, A., Guo, J., Sienkiewicz, M., and Lamich, D.: Assessing the effects of data selection with the DAO physical-space statistical analysis system, Mon. Weather Rev., 126, 2913–2926, 1998.

Collins, N., Theurich, G., DeLuca, C., Suarez, M., Trayanov, A., Balaji, V., Li, P., Yang, W., Hill, C., and da Silva, A.: Design and implementation of components in the Earth System Mod-

ACPD
12, 9985–10014, 2012

eling Framework, Int. J. High Perform. C., 19, 341–350, doi:10.1177/1094342005056120, 2005.
Corbin, K. D. and Denning, A. S.: Using continuous data to estimate clear-sky errors in inversions of satellite CO_2 measurements, Geophys. Res. Lett., 33, L12810, doi:10.1029/2006GL025910, 2006.
Corbin, K. D., Denning, A. S., Wang, J.-W., Lu, L., Prihodko, L., and Baker, I. T.: Possible representation errors in inversions of satellite CO_2 retrievals, J. Geophys. Res., 113, D02301, doi:10.1029/2007JD008716, 2008.
Crisp, D., Fisher, B. M., O'Dell, C., Frankenberg, C., Basilio, R., Bösch, H., Brown, L. R., Castano, R., Connor, B., Deutscher, N. M., Eldering, A., Griffith, D., Gunson, M., Kuze, A., Mandrake, L., McDuffie, J., Messerschmidt, J., Miller, C. E., Morino, I., Natraj, V., Notholt, J., O'Brien, D. M., Oyafuso, F., Polonsky, I., Robinson, J., Salawitch, R., Sherlock, V., Smyth, M., Suto, H., Taylor, T. E., Thompson, D. R., Wennberg, P. O., Wunch, D., and Yung, Y. L.: The ACOS CO_2 retrieval algorithm – Part II: Global X_{CO_2} data characterization, Atmos. Meas. Tech., 5, 687–707, doi:10.5194/amt-5-687-2012, 2012.
Denning, A. S., Holzer, M., Gurney, K. R., Heimann, M., Law, R. M., Rayner, P. J., Fung, I. Y., Fan, S., Taguchi, S., Friedlingstein, P., Balkanski, Y., Taylor, J., Maiss, M., and Levin, I.: Three-dimensional transport and concentration of SF6: A model intercomparison study (TransCom 2), Tellus B, 51, 266–297, 1999.
Eguchi, N. and Yokota, T.: Investigation of clear-sky occurrence rate estimated from CALIOP and MODIS observations, Geophys. Res. Lett., 35, L23816, doi:10.1029/2008GL035897, 2008.
Gurney, K., Law, R. M., Denning, A. S., Rayner, P. J., Baker, D., Bousquet, P., Bruhwiler, L., Chen, Y.-H., Ciais, P., Fan, S., Fung, I. Y., Gloor, M., Heimann, M., Higuchi, K., John, J., Maki, T., Maksyutov, S., Masarie, K., Peylin, P., Prather, M., Pak, B. C., Randerson, J., Sarmiento, J., Taguchi, S., Takahashi, T., and Yuen, C.-W.: Towards robust regional estimates of CO_2 sources and sinks using atmospheric transport models, Nature, 415, 626–630, 2002.
Hack, J. J.: Parameterization of moist convection in the National Center for Atmospheric Research community climate model (CCM2), J. Geophys. Res., 99, 5551–5568, 1994.
Holtslag, A. A. M. and Boville, B. A.: Local versus non-local boundary layer diffusion in a global climate model, J. Climate, 6, 1825–1842, 1993.
Houweling, S., Aben, I., Breon, F.-M., Chevallier, F., Deutscher, N., Engelen, R., Gerbig, C., Griffith, D., Hungershoefer, K., Macatangay, R., Marshall, J., Notholt, J., Peters, W., and Serrar,

ACPD
12, 9985–10014, 2012

S.: The importance of transport model uncertainties for the estimation of CO_2 sources and sinks using satellite measurements, Atmos. Chem. Phys., 10, 9981–9992, doi:10.5194/acp-10-9981-2010, 2010.

Kang, J. S., Kalnay, E., Liu, J., Fung, I., Miyoshi, T., and Ide, K.: "Variable localization" in an ensemble Kalman filter: Application to the carbon cycle data assimilation, J. Geophys. Res., 116, D09110, doi:10.1029/2010JD014673, 2011.

Kawa, S. R., Erickson III, D. J., Pawson, S., and Zhu, Z.: Global CO_2 transport simulations using meteorological data from the NASA data assimilation system, J. Geophys. Res., 109, D18312, doi:10.1029/2004JD004554, 2004.

Kiehl, J. T., Hack, J. J., Bonan, G. B., Boville, B. A., Williamson, D. L., and Rasch, P. J.: The National Center for Atmospheric Research Community Climate Model: CCM3, J. Climate, 11, 1131–1149, 1998.

Kuze, A., Suto, H., Nakajima, M., and Hamazaki, T.: Thermal and near infrared sensor for carbon observation Fourier-transform spectrometer on the Greenhouse Gases Observing Satellite for greenhouse gases monitoring, Appl. Optics, 48, 6716–6733, doi:10.1364/AO.48.006716, 2009.

Lauvaux, T., Pannekoucke, O., Sarrat, C., Chevallier, F., Ciais, P., Noilhan, J., and Rayner, P. J.: Structure of the transport uncertainty in mesoscale inversions of CO_2 sources and sinks using ensemble model simulations, Biogeosciences, 6, 1089–1102, doi:10.5194/bg-6-1089-2009, 2009.

Law, R. M., Chen, Y.-H., Gurney, K. R., and TransCom 3 Modellers: TransCom 3 CO_2 inversion intercomparison: 2. Sensitivity of annual mean results to data choices, Tellus B, 55, 580–595, 2003.

Lin, S.-J.: A "Vertically Lagrangian" finite-volume dynamical core for global models, Mon. Weather Rev., 132, 2293–2307, 2004.

Liu, J., Fung, I., Kalnay, E., and Kang, J.-S.: CO_2 transport uncertainties from the uncertainties in meteorological fields, Geophys. Res. Lett., 38, L12808, doi:10.1029/2011GL047213, 2011.

Lock, A. P., Brown, A. R., Bush, M. R., Martin, G. M., and Smith, R. N. B.: A new boundary layer mixing scheme. Part I: Scheme description and single-column model tests, Mon. Weather Rev., 138, 3187–3199, 2000.

ACPD
12, 9985–10014, 2012

Lokupitiya, R. S., Zupanski, D., Denning, A. S., Kawa, S. R., Gurney, K. R., and Zupanski, M.: Estimation of global CO_2 fluxes at regional scale using the maximum likelihood ensemble filter, J. Geophys. Res., 113, D20110, doi:10.1029/2007JD009679, 2008.

Louis, J., Tiedtke, M., and Geleyn, J.: A short history of the PBL parameterization at ECMWF, Proc. ECMWF Workshop on Planetary Boundary Layer Parameterization, Reading, United Kingdom, ECMWF, 59–80, 1982.

Moorthi, S. and Suarez, M. J.: Relaxed Arakawa-Schubert: A parameterization of moist convection for general circulation models, Mon. Weather Rev., 120, 978–1002, 1992.

Ott, L. E., Bacmeister, J., Pawson, S., Pickering, K., Stenchikov, G., Suarez, M., Huntrieser, H., Loewenstein, M., Lopez, J., and Xueref-Remy, I.: Analysis of convective transport and parameter sensitivity in a single column version of the Goddard earth observation system, version 5, general circulation model, J. Atmos. Sci., 66, 627–646, 2009.

Parazoo, N. C., Denning, A. S., Kawa, S. R., Corbin, K. D., Lokupitiya, R. S., and Baker, I. T.: Mechanisms for synoptic variations of atmospheric CO_2 in North America, South America and Europe, Atmos. Chem. Phys., 8, 7239–7254, doi:10.5194/acp-8-7239-2008, 2008.

Parazoo, N. C., Denning, A. S., Berry, J., Wolf, A., Randall, D., Kawa, S. R., Pauluis, O., Doney, S. C.: Moist synoptic transport of CO_2 along the mid-latitude storm track, 38, L09804, doi:10.1029/2011GL047238, 2011.

Pawson, S., Stajner, I., Kawa, S. R., Hayashi, H., Tan, W.-W., Nielsen, J. E., Zhu, Z., Chang, L.-P., and Livesey, N. J.: Stratospheric transport using 6-h-averaged winds from a data assimilation system, J. Geophys. Res., 112, D23103, doi:10.1029/2006JD007673, 2007.

Peylin, P., Bousquet, P., Le Quere, C., Sitch, S., Friedlingstein, P., McKinley, G., Gruber, N., Rayner, P., and Ciais, P.: Multiple constraints on regional CO_2 flux variations over land and oceans, Global Biogeochem. Cy., 19, GB1011, doi:10.1029/2003GB002214, 2005.

Rienecker, M. M., Suarez, M. J., Todling, R., Bacmeister, J., Takacs, L., Liu, H.-C., Gu, W., Sienkiewicz, M., Koster, R. D., Gelaro, R., Stajner, I., and Nielsen, E.: The GEOS-5 Data Assimilation System-Documentation of versions 5.0.1 and 5.1.0, and 5.2.0. NASA Tech. Rep. Series on Global Modeling and Data Assimilation, NASA/TM-2008-104606, Vol. 27, 92 pp., 2008.

Rienecker, M. M., Suarez, M. J., Gelaro, R., Todling, R., Bacmeister, J., Liu, E., Bosilovich, M. G., Schubert, S. D., Takacs, L., Kim, G. K., Bloom, S., Chen, J., Collins, D., Conaty, A., da Silva, A., Gu, W., Joiner, J., Koster, R. D., Lucchesi, R., Molod, A., Owens, T., Pawson, S., Pegion, P., Redder, C. R., Reichle, R., Robertson, F. R., Ruddick, A. G., Sienkiewicz,

ACPD
12, 9985–10014, 2012

M., and Woollen, J.: MERRA: NASA's Modern-Era Retrospective Analysis for Research and Applications, J. Climate, 24, 3624–3648, doi:10.1175/JCLI-D-11-00015.1, 2011.
Schuh, A. E., Denning, A. S., Corbin, K. D., Baker, I. T., Uliasz, M., Parazoo, N., Andrews, A. E., and Worthy, D. E. J.: A regional high-resolution carbon flux inversion of North America for 2004, Biogeosciences, 7, 1625–1644, doi:10.5194/bg-7-1625-2010, 2010.
Stephens, B. B. Gurney, K. R., Tans, P. P., Sweeney, C., Peters, W., Bruhwiler, L., Ciais, P., Ramonet, M., Bousquet, P., Nakazawa, T., Aoki, S., Machida, T., Inoue, G., Vinnichenko, N., Lloyd, J., Jordan, A., Heimann, M., Shibistova, O., Langenfelds, R. L., Steele, L. P., Francey, R. J., and Denning, A. S.: Weak northern and strong tropical land carbon Uptake from vertical profiles of atmospheric CO_2, Science, 316, 1732–1735, 2007.
Teixeira, J. and Reynolds, C. A.: Stochastic nature of physical parameterization in ensemble prediction: A stochastic convection approach, Mon. Weather Rev., 136, 483–496, doi:10.1175/2007MWR1870.1, 2008.
Wu, W.-S., Purser, R. J., and Parrish, D. F.: Three-Dimensional Variational Analysis with Spatially Inhomogeneous Covariances, Mon. Weather Rev., 130, 2905–2916, 2002.
Yang, Z., Washenfelder, R. A., Keppel-Aleks, G., Krakauer, N. Y., Randerson, J. T., Tans, P. P., Sweeney, C., and Wennberg, P. O.: New constraints on Northern Hemisphere growing season net flux, Geophys. Res. Lett., 34, L12807, doi:10.1029/2007GL029742, 2007.
Yi, C., Davis, K. J., Bakwin, P. S., Denning, A. S., Zhang, N., Desai, A., Lin, J. C., and Gerbig, C.: Observed covariance between ecosystem carbon exchange and atmospheric boundary layer dynamics at a site in northern Wisconsin, J. Geophys. Res., 109, D08302, doi:10.1029/2003JD004164, 2004.
Zhang, G. J. and McFarlane, N. A.: Sensitivity of climate simulations to the parameterization of cumulus convection in the Canadian climate center general-circulation model, Atmos. Ocean, 33, 407–446, 1995.
Zupanski, D., Denning, A. S., Uliasz, M., Zupanski, M., Schuh, A. E., Rayner, P. J., Peters, W., and Corbin, K. D.: Carbon flux bias estimation employing Maximum Likelihood Ensemble Filter (MLEF), J. Geophys. Res., 112, D17107, doi:10.1029/2006JD008371, 2007.

ACPD
12, 9985–10014, 2012

Table 1. Description of meteorological datasets used in offline tracer transport simulations. Column 1 (data) is the code name for the meteorological dataset, 2 (version) is the version of the analysis product, 3 (native resolution) is the resolution at which the analysis system (forecast + assimilation) is run ($a \times b \times c$ = latitude spacing × longitude spacing × number of vertical levels), 4 (transport resolution) is the grid spacing at which the analysis is saved, 5 (full or reduced) refers to whether the analysis is saved at the native resolution of the parent GCM or interpolated to a coarser resolution, 6 (deep convection) is the deep convection scheme of the parent GCM, and 7 (turbulence) is the PBL turbulence scheme of the parent GCM. Naming convention for analysis product in the first column is as follows: character 1–2 is the product version number (G4 = GEOS-4 and G5 = GEOS-5), character 3 is the grid at which the analysis is saved (F = full resolution and R = reduced resolution), and character 4–5 is the latitude grid spacing at which the analysis is saved for offline transport (05 = 0.5°, 10 = 1.0°, 20 = 2.0°).

Run	Version	Native resolution	Transport resolution	Full or reduced	Deep convection	Turbulence
G5F05	5.1.0	0.5° × 0.67° × 72	0.5° × 0.67° × 42	Full	Moorthi and Suarez (1992)	Louis et al. (1982) Lock et al. (2000)
G5R10	5.2.0	0.5° × 0.67° × 72	1.25° × 1.0° × 42	Reduced (regridded from G5F05)	Moorthi and Suarez (1992)	Louis et al. (1982) Lock et al. (2000)
G4F10	4.5.3	1.25° × 1.0° × 55	1.25° × 1.0° × 25	Full	Zhang and McFarlane (1995)	Holtslag and Boville (1993)
G4R20	4.5.3	1.25° × 1.0° × 55	2.5° × 2.0° × 25	Reduced (regridded from G4F10)	Zhang and McFarlane (1995)	Holtslag and Boville (1993)

ACPD
12, 9985–10014, 2012

Table 2. Summary of OSSE's used in source/sink inversions. Red shading refers to "perfect transport" experiments, green "signal detection", and blue "biased transport". The "true" flux refers to the set of surface CO_2 fluxes prescribed in Step 1. The "prior" flux refers to surface fluxes used as a first guess in Step 2. Prior fluxes are described in Parazoo et al. (2008), and include a steady state terrestrial biosphere. This means that the true flux in Experiments 1, 2 and 5 is the same as the prior flux used in Step 2, while the true flux in Experiments 3, 4 and 6 also includes a globally distributed 3 GtC sink (see Fig. 7a).

Experiment	Observation transport (Step 1)	Inversion transport (Step 2)	True flux	Cloud screening
1	GEOS-4	GEOS-4	Prior	No
2	GEOS-4	GEOS-4	Prior	Yes
3	GEOS-4	GEOS-4	Prior + Constant 3 GtC Sink	Yes
4	GEOS-4	GEOS-4	Prior + Seasonal 3 GtC Sink	Yes
5	GEOS-5	GEOS-4	Prior	Yes
6	GEOS-5	GEOS-4	Prior + Seasonal 3 GtC Sink	Yes

ACPD
12, 9985–10014, 2012

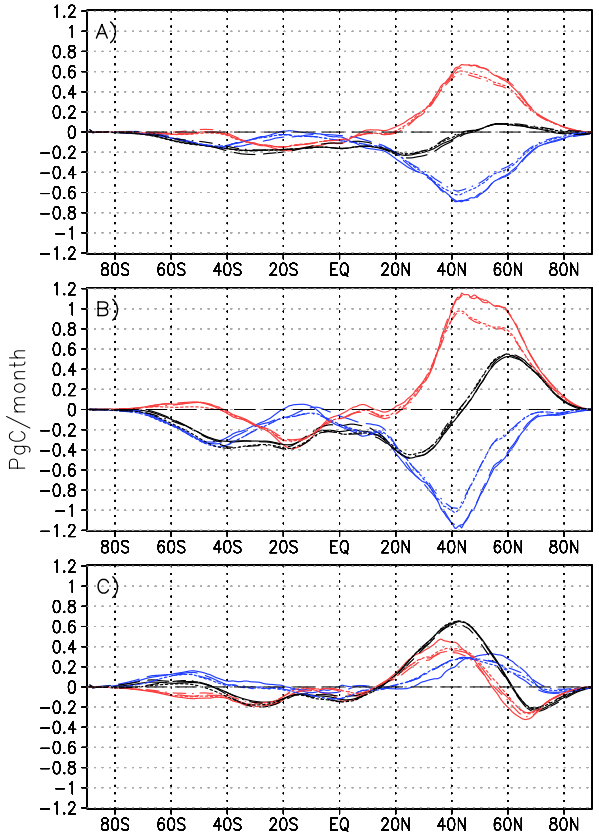

Fig. 1. Zonal-mean column integrated meridional CO_2 transport averaged over **(A)** 1 yr, **(B)** December-January-February and **(C)** June-July-August. Total meridional transport is shown in black, "mean" transport in blue, and "eddy" transport in red. Line styles correspond to transport by the four meteorological analyses, where G5F05 is solid, G5R10 is dashed, G4F10 is dotted, and G4R20 dash-dotted.

ACPD
12, 9985–10014, 2012

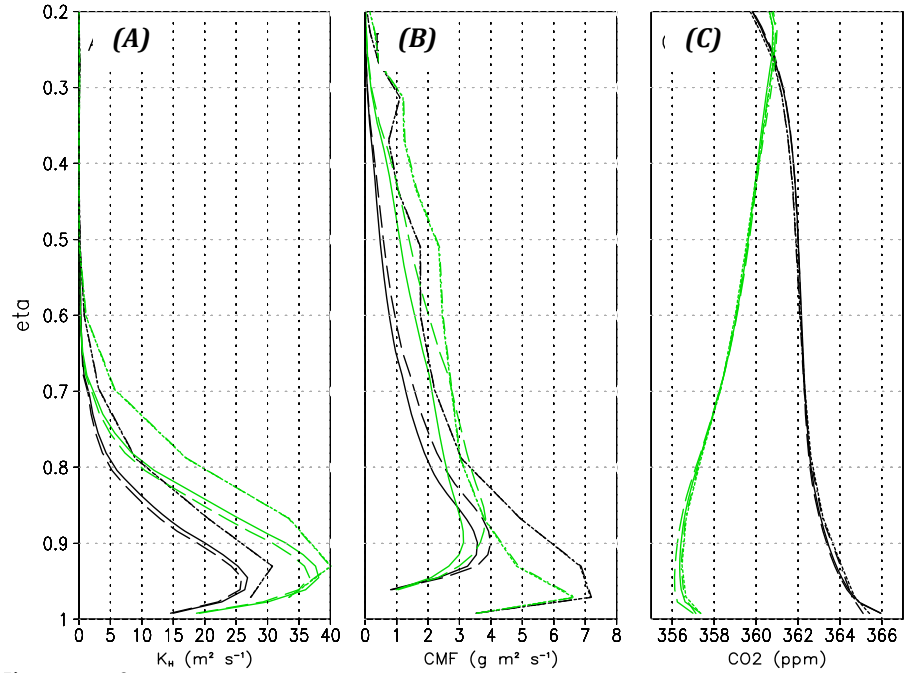

Fig. 2. Vertical profiles of **(A)** turbulent diffusion, **(B)** cumulus mass flux and **(C)** CO_2 mixing ratio, zonally averaged, binned into mid-latitudes (30–70° N) and plotted as a function of the terrain following coordinate eta for each of the four meteorological analyses (line styles correspond to Fig. 1). Annual averages are plotted in black, summer averages in green. Mass fluxes from GEOS-4 are identical and therefore lie directly over one another.

ACPD
12, 9985–10014, 2012

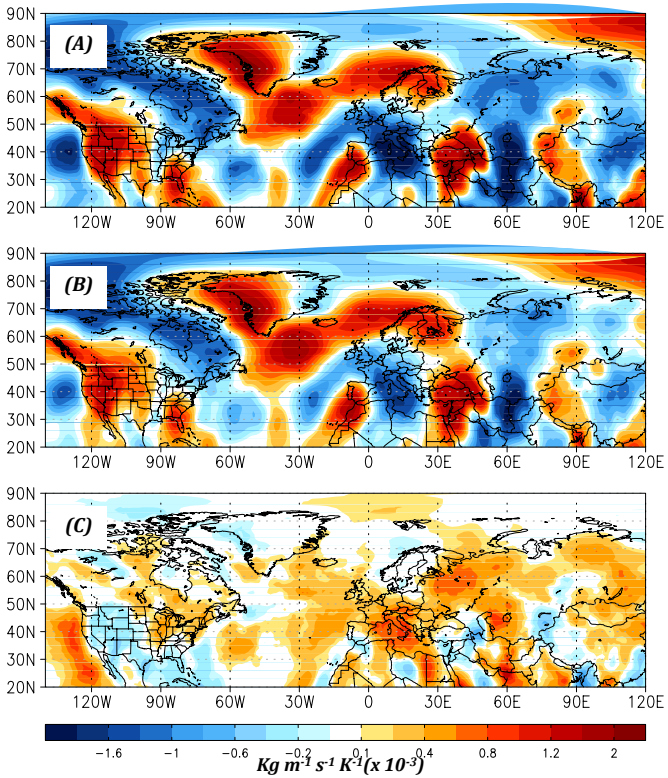

Fig. 3. Spatial structure of column averaged meridional mass flux averaged during the period June-July-August for **(A)** G4R20 and **(B)** G5F05. **(C)** The difference in meridional mass flux, or **(B)** minus **(A)**.

ACPD
12, 9985–10014, 2012

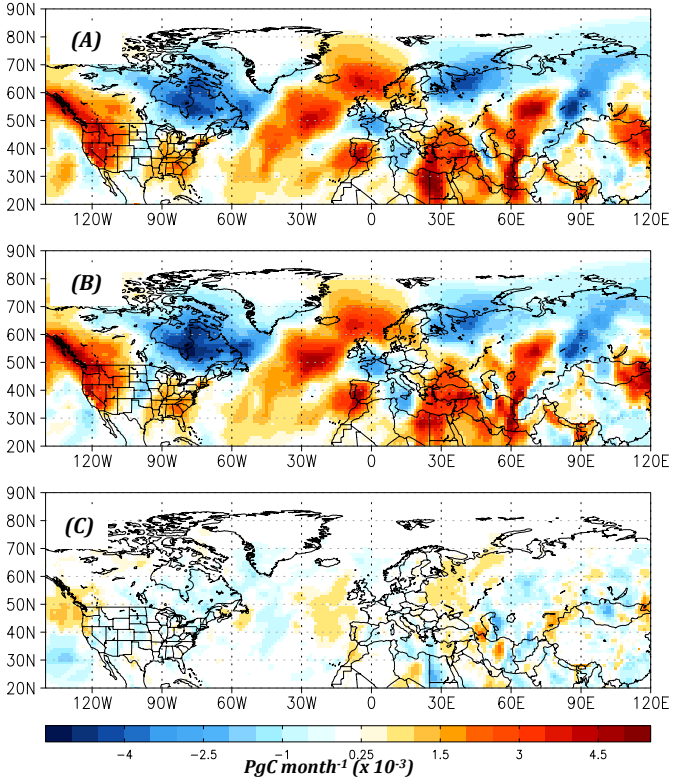

Fig. 4. Spatial structure of column integrated eddy CO_2 transport averaged over the period June-July-August for **(A)** G4R20 and **(B)** G5F05. **(C)** Difference in eddy transport, or **(B)** minus **(A)**.

ACPD
12, 9985–10014, 2012

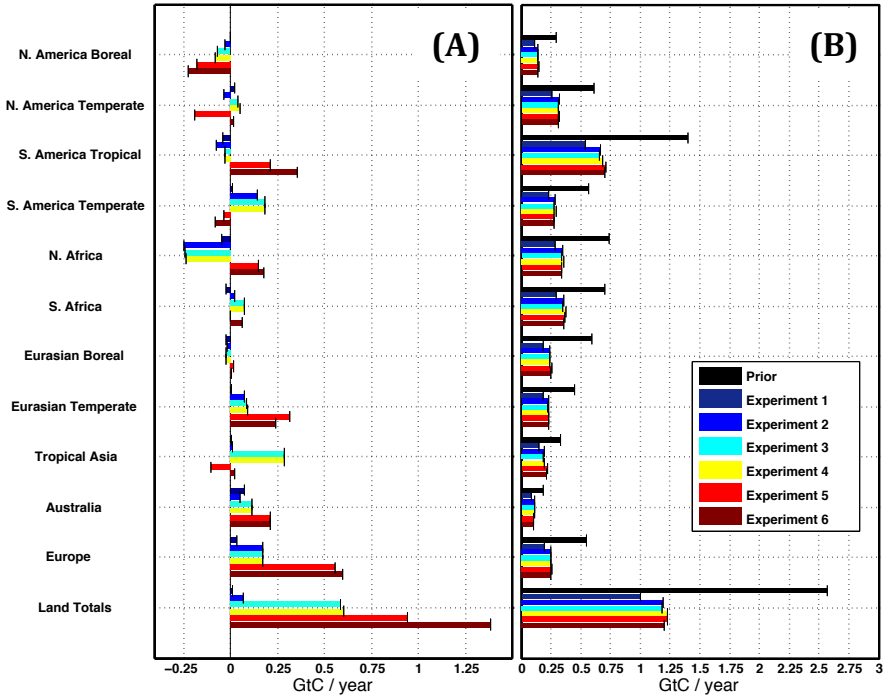

Fig. 5. Bar plots of total annual terrestrial flux error **(A)** and uncertainty **(B)** for Experiments 1–6, aggregated up to regional and global scale.

ACPD
12, 9985–10014, 2012

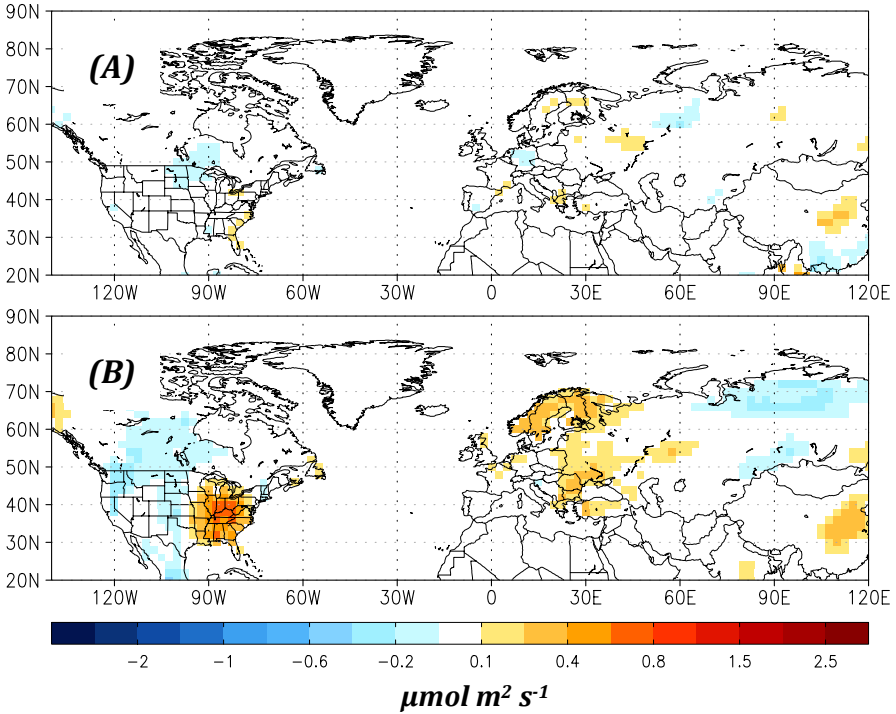

Fig. 6. Flux errors during boreal summer (June-July-August) in **(A)** Experiment 1 and **(B)** Experiment 2.

ACPD
12, 9985–10014, 2012

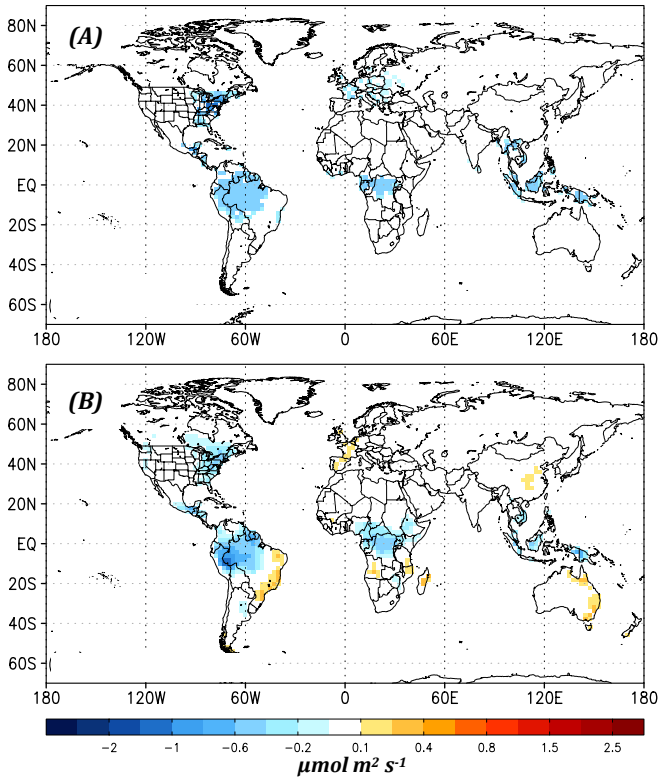

Fig. 7. (A) True and **(B)** recovered fluxes for Experiment 3, averaged over one year.

ACPD
12, 9985–10014, 2012

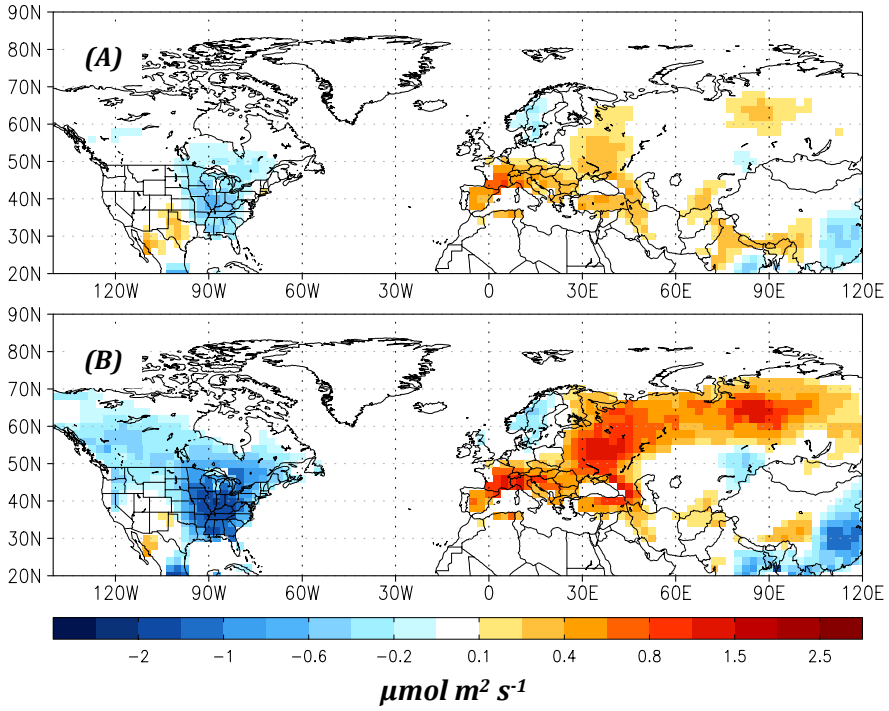

Fig. 8. Flux "errors" in Experiment 5, averaged over **(A)** 1 yr and **(B)** June-July-August.

ACPD
12, 9985–10014, 2012